International Journal of Mechanical and Electrical Engineering
ISSN: 3005-9615 (Print), ISSN: 3005-7132 (Online) | Volume 5, Number 2, Year 2025
DOI: https://doi.org/10.62051/ijmee.v5n2.03
Journal homepage: https://wepub.org/index.php/IJMEE/index

Effect of Laser Power on the Organization and Properties of NiCrFeCu-45%WC Composite Cladding Layer

Junpeng Sun [1, 2, 3], Shufeng Sun [1, 2, 3, *], Mingsai Zhang [1, 2, 3], Yanyan Song [1, 2, 3], Liang Li [1, 2, 3]

[1] Discipline innovation and Wisdom Introduction Base of High-end Laser Intelligent Manufacturing Technology and Equipment, Qingdao University of Technology, Qingdao 266525, China
[2] Shandong Provincial Key Laboratory of Laser Green Intelligent Manufacturing Technology, Qingdao University of Technology, Qingdao. 266525, China
[3] School of Qingdao Technological university, Qingdao 266520, China
* Corresponding Author: Shufeng Sun (Email: sunshufeng@qut.edu.cn)

ABSTRACT

In order to improve the wear resistance of 42CrMo steel for rock drill bits, NiCrFeCu-45%WC composite cladding layer was prepared by laser cladding technology, and the influence of laser power at 1500W-1800W on the organization evolution and mechanical properties of the cladding layer was systematically investigated. The XRD, SEM/EDS and friction wear tests show that the physical phase of the cladding layer is dominated by γ-(Ni,Fe) solid solution, accompanied by the formation of WC, W_2C and $Cr_{23}C_6/M_7C_3$ carbides. When the power was increased to 1600 W, the trace WC decomposed into W_2C particles, and the grains remained small in size due to heterogeneous nucleation and Zener pinning effect, and the microhardness of the cladding layer reached a peak (average 747.6 $HV_{1.0}$), which was 1.4 times higher than that of the substrate, and at this time, the wear rate was at a minimum of 1.6×10^{-2} mm^3/Nm. The study showed that the The optimal wear resistance of the cladding layer at 1600 W is achieved through fine grain strengthening, hard phase dispersion and carbide synergism.

KEYWORDS

Laser Cladding; Drill Bit; Ni-WC Coating; Phase Composition; Microstructure; Wear Resistance.

1. INTRODUCTION

42CrMo steel, the main material for rock drill bit manufacturing, is characterized by high hardness, high strength, good hardenability and low price [1,2]. Therefore, improving the hardness and wear resistance of the braze head becomes an important step to promote the high-end development of rock drilling machinery. Laser cladding a good surface modification technology. The appearance of nickel-based alloy and tungsten carbide ceramic composite cladding layer can be a stable combination of the strong toughness of the metal and the excellent wear resistance of ceramics [3,4].Zhao et al [5] used laser cladding technology to prepare Ni-based alloy and different content of WC for functional gradient multilayer cladding. The results showed that no cracks appeared in the cladding layer due to the alleviation of the differences in the thermal expansion coefficients of the layers.Bartkowski D[6] et al. prepared Fe-based alloy-WC composite cladding layer, and the study showed that the optimization of the process parameters can effectively improve the wear and corrosion resistance of the cladding layer.Li et al.[7] studied the strengthening mechanism of Inconel 625 composite cladding

layer by spherical WC and non-spherical WC. Inconel 625 composite cladding layer. The results show that spherical WC has better wear resistance.When the content of WC in the composite cladding layer is too high, due to the differences in material toughness and coefficient of thermal expansion, cracks and other defects are easily produced during the cladding process, while NiCrFeCu alloy has been re-proportioned on the basis of traditional nickel-based alloys in terms of material elements and content, and the addition of Cu elements significantly improves the toughness of the material to inhibit the production of cracks.

In this paper, to strengthen the brazing head wear-resistant performance as the goal, using laser cladding technology by controlling the laser power in the brazing head material 42CrMo steel substrate prepared high hard wear-resistant NiCrFeCu-45% WC composite cladding layer, analysis of the composition of the physical phase of the cladding layer under different laser power, microstructure of the evolution of the law and mechanism, as well as the hardness and wear-resistant influence of the law.

2. EXPERIMENTAL MATERIALS AND METHODS

Experimentally, 42CrMo steel, which is commonly used for rock drill bits, was selected as the matrix material, and its main chemical elements are shown in Table 1. The cladding layer powder is NiCrFeCu-45% WC composite powder, the main chemical element composition as shown in Table 2, mainly spherical particles, with good wettability, mobility, particle size of 50~150um, powder morphology as shown in Figure 1. The alloy powder was preset on the surface of the substrate to form a powder bed of 1mm×10mm×50mm, and then dried for 120min using a drying oven at a set temperature of 100 ℃ to remove the moisture in the mixed powder to prevent affecting the effect of the cladding layer and the quality of the cladding layer.

The experiments were conducted using a FL020 fiber laser with a maximum power of 2kW for laser cladding. After the pre-experiment, the laser power variable, the variation interval is 1500W-1800W, and the rest of the parameters are unchanged as shown in Table 3. The surface of the cladding was polished and cleaned with ultrasonic waves for 20 min, and the specimens were corroded in aqua regia solution for 20 s. The microstructure of the cladding was analyzed using SEM observation and the elemental compositions and distributions were measured using the EDS function. X-ray diffractometer was used to measure the physical composition of the cladding layer. The hardness was measured by HV-1000 microhardness tester. The parameters of the friction wear test were set as follows: frequency setting 2Hz, unidirectional displacement 6mm, load 20N, time 20min, and laser confocal microscope was used to measure the three-dimensional contour of the worn specimen and calculate the wear volume.

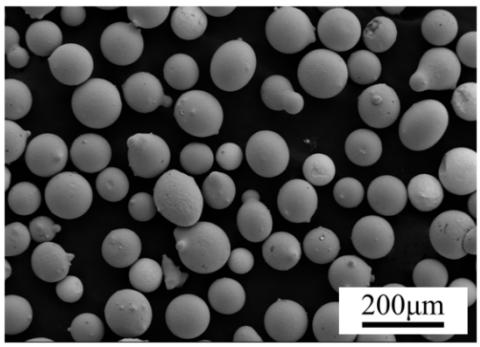

Figure 1. Morphology of NiCrFeCu-45%WC powder

Table 1. Main chemistry of 42CrMo steel

Element	C	Cr	Mn	Si	Mo	Fe
Wt.%	0.42%	0.12%	0.65%	0.28%	0.22%	Bal.

Table 2. Main chemistry of NiCrFeCu-45%WC alloy particles

Element	O	Cr	Fe	Cu	W	C	Ni
Wt.%	0.058	15.6	5.5	2.2	45.2	3.21	Bal.

Table 3. Technology parameters

Parameter	Spot diameter	Scanning speed	Protective gas flow rate
Parameter value	3mm	4mm/s	6L/min

3. RESULTS AND DISCUSSION

3.1. Cross-sectional Morphology

Figure 2 shows the cross-sectional morphology of the cladding layer under different laser powers. As can be seen from the figure, no defects such as cracks and porosity were found in the cladding layer, and it showed good metallurgical bonding with the substrate. With the change of laser power, there is no significant change in the dilution rate, indicating that the heat input of the melt pool and the heat conduction of the substrate have reached a dynamic equilibrium. Combined with the microstructure analysis of the molten cladding layer in Figure 5, it was found that when the power was raised to more than 1700 W, the grains in the heat-affected zone of the molten cladding layer and the substrate were slightly roughened, which might be related to the local heat accumulation. From the figure, it can be observed that the bright and dark phase regions of each cross-section are distinct, combined with the elemental analysis in Figure 4, which shows that the bright-phase components are WC particles, and the dark-phase components are mainly nickel-based alloys. The WC particles are distributed in the cladding layer, and as a hard phase, they can play the role of diffusion reinforcement for the cladding layer. The WC particles were uniformly distributed in the cladding layer under the convection of Marangoni, and there was no obvious bias aggregation or burnout, which indicated that the laser power was well matched with the flow of the molten pool.

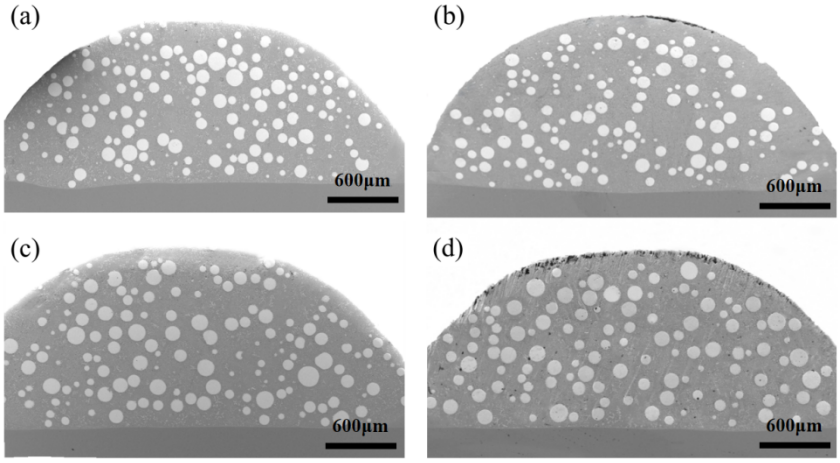

Figure 2. Cross-sectional view of the cladding layers:
(a) 1500W, (b) 1600W, (c) 1700W, (d) 1800W

3.2. Composition of the Physical Phase of the Cladding Layer

As shown in Figure 3, the XRD test patterns of NiCrFeCu-45%WC composite cladding layers at different laser powers are shown. After calibration of the physical phases, it was found that the cladding layers were mainly dominated by γ-(Ni,Fe) solid solution, Ni-Cr-Fe, $Cr_{23}C_6$, M_7C_3 (M=Fe, Cr), WC, W_2C, and $FeNi_3$ physical phases.

Each cladding layer is dominated by γ-(Ni,Fe) solid solution, Ni-Cr-Fe solid solution and $FeNi_3$ intermetallic compounds coexist. When the power is 1500W, the power is lower, the diffraction peak of γ-(Ni,Fe) solid solution is wider, which indicates that the grain size is smaller and the lattice distortion is significant, which may be related to the rapid non-equilibrium solidification of solid solution caused by insufficient energy of the melting pool, and the WC diffraction peak is high and the W_2C phase is not detected, which indicates that the WC is not decomposed in the low-temperature melting pool, and the diffraction peaks of $Cr_{23}C_6$ and M_7C_3 are significant, which indicates that the low-temperature environment of the melting pool is more favorable for Cr/Fe intermetallic compound. The significant diffraction peaks of $Cr_{23}C_6$ and M_7C_3 indicate that the low-temperature environment of the molten pool is more favorable for the combination of Cr/Fe and C. When the power is 1600W, the intensity of WC peaks is detected to decay, and W_2C diffraction peaks appear at the same time. This indicates that the partial decomposition reaction is initiated at this time:

$$WC \rightarrow W_2C+CWC \rightarrow W_2C+C \quad (1)$$

However, the diffraction peak of γ-(Ni,Fe) solid solution is still broad, which indicates that the grain size has not changed significantly. After the power greater than 1700 W, due to the high power, γ-(Ni,Fe) diffraction peaks sharpened, grain size increased, WC peak intensity and W2C diffraction peak intensity did not appear obvious changes, but $Cr_{23}C_6$, M_7C_3 peak intensity is relatively lower, analyze the reasons for this may be related to the high temperature of the carbon activity increases, Cr/Fe element solid solubility increases, Cr, Fe atoms at high temperatures, diffusion The reason may be related to the increase of carbon activity and solid solubility of Cr/Fe elements at high temperatures, and the increase of diffusion of Cr and Fe atoms at high temperatures. The related phases of Cu were not detected in all control groups, and Cu elements may be distributed in the γ-(Ni,Fe) lattice when analyzed by EDS, which is due to the similarity of lattice parameters between Cu and Ni, which preferentially forms a replacement solid solution.

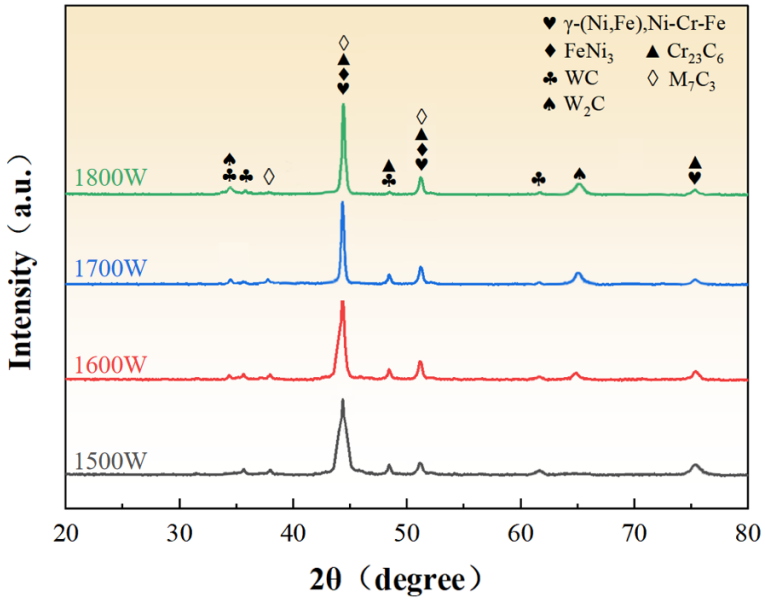

Figure 3. XRD pattern of the cladding layer at laser power of 1500W-1800W

3.3. Element Distribution and Microstructure of the Cladding Layer

Figure 4 shows the morphology of the in situ precipitated phases and their distribution of important elements in each layer under different powers. When the laser power is 1500 W, the W elements are highly concentrated in the region of the unmelted WC particles, and there are almost no W elements present in the nickel-based alloys, which suggests that the melting pool temperature is not enough to trigger the decomposition of WC particles or the diffusion of W atoms. However, with the increasing laser power, when the laser power reaches more than 1600 W, as shown in Figure 4(b), (c), and (d), the W element in the nickel-based alloy increases, and combined with the XRD detection results, the W_2C phase is found to be generated. This indicates that the molten pool temperature exceeds the WC decomposition threshold at high power. When the power was increased to 1800 W, a diffusion band of W elements appeared at the edge of WC particles, but the particles were still dominated by mechanical embedding rather than metallurgical reactions. In addition, the EDS surface scan shows that the O-element content gradually increases with the power increase, and at 1800 W, localized O-element agglomeration occurs (Fig. 4d), which may be attributed to the high temperature of the molten pool exacerbating the plasma perturbation, leading to the failure of the protective gas layer and oxidation reaction in some regions. However, no oxide phase was detected by XRD, and it is presumed that the oxides are diffusely distributed in the form of amorphous or nanoparticles.

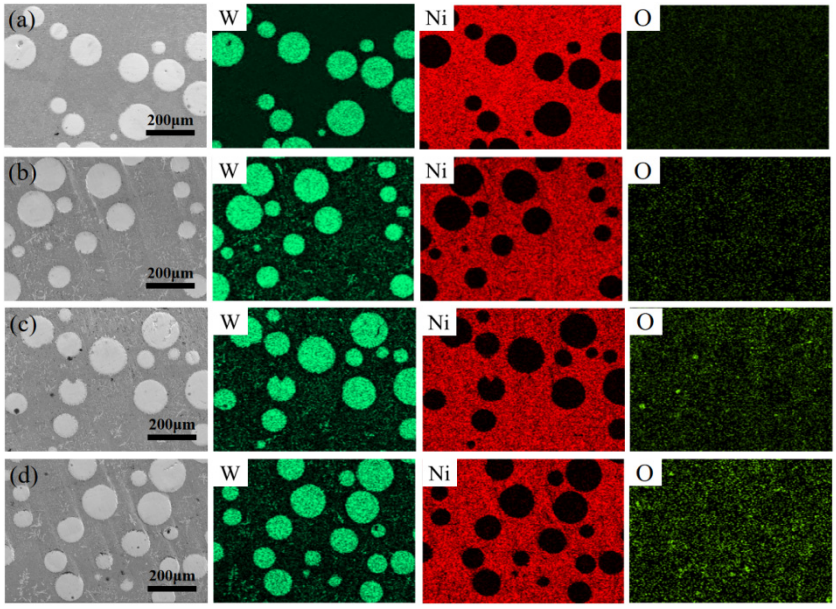

Figure 4. Microstructure and elemental distribution of the cladding layer:

(a) 1500W, (b) 1600W, (c) 1700W, (d) 1800W

Figure 5 shows the evolution of microstructure of each cladding layer at 1500W-1800W. Through comparison, it is found that the grain size is similar between the laser power of 1500W and 1600W, the reason for this is that at 1500W, the molten pool energy loss is low, the molten pool volume is small, the cooling rate is fast, and the grains are dominated by fine cytosine crystals; although the power rises at 1600W, but the grain size is not significantly roughened, which is a result of the combination of the thermal equilibrium and a variety of effects: (1) the heat input of the molten pool and the cooling rate reach a dynamic equilibrium, suppressing the excessive growth of γ-(Ni,Fe) grains. This is the result of a combination of thermal equilibrium and various effects: (1) The heat input to the molten pool and the cooling rate reach a dynamic equilibrium, which inhibits the excessive growth of γ-(Ni,Fe) grains. (2) heterogeneous nucleation effect (3) grain boundary pinning effect. However, when the power reaches 1700W, with the power to increase the size of the cytosolic crystals increased rapidly and the emergence of thick dendritic arms, analyze the reasons may be the following: (1) high power melt pool volume increases, the cooling rate decreases which will make

the melt pool high temperature zone expansion, low cooling rate, the dendritic crystal growth mode dominates, the size of the grains increased significantly. (2) The rapid solidification of the molten pool under high power triggers the accumulation of thermal stresses, which are concentrated at the grain boundaries during the cooling process of the molten pool, inducing the migration of the grain boundaries and the merging of the grains.

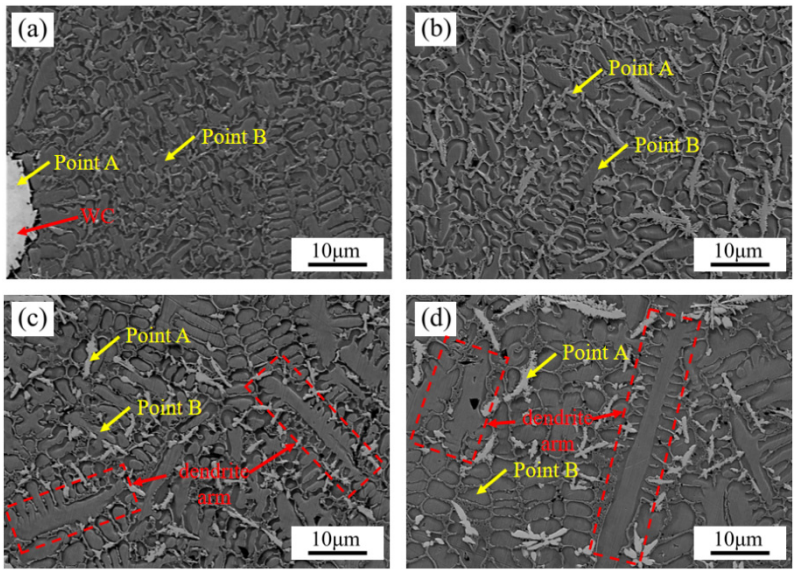

Figure 5. Microstructure of the cladding layers: (a) 1500W, (b) 1600W, (c) 1700W, (d) 1800W

3.4. Hardness

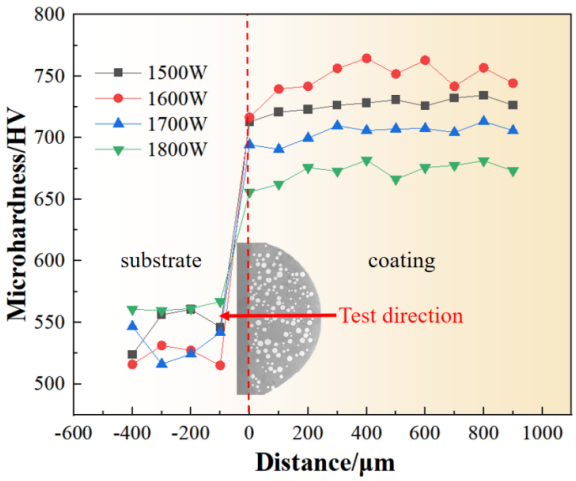

Figure 6. Microhardness distribution of the cladding layers cross-section

As shown in Figure 6, the microhardness (ignoring the WC particle data) characterization of the cladding layers prepared with different laser powers reveals that the top of the cladding layer has the highest hardness, which gradually decreases toward the substrate. In addition to the dilution effect of the substrate on the molten cladding layer at the bottom, other reasons were carefully analyzed: (1) grain size gradient effect, the same molten cladding layer with the depth of the deeper, there is a tendency for the grain size to become larger, and even the growth of the emergence of a thick dendritic arm. This is because the top region of the cladding layer is favorable for heat release, and the top solidifies rapidly, forming fine grains, which can be seen through the Hall-Petch relationship [8], and the hardness is significantly enhanced by the refinement of the grains. While the region close to the substrate decreases the cooling rate due to the accumulation of heat transfer, and the coarsening of the grains leads to a decrease in hardness by about. (2) Due to elemental diffusion, the top $Cr_{23}C_6$ and

M_7C_3 carbides are synergistically strengthened with γ-(Ni,Fe) solid solution, causing lattice distortion and enhancing hardness. And with the increase of depth, the diffusion of Fe and Cr elements at the interface leads to the decrease of stability of γ-(Ni,Fe) solid solution, while the decrease of carbide content also leads to the decrease of carbide precipitation and the decrease of hardness.

3.5. Abrasion Resistance of the Cladding Layer

The coefficient of friction of the 42CrMo steel substrate and the cladding layers was measured, which is an important indicator of the wear resistance of the material under complex working conditions, and the lower the value, the stronger the wear resistance means, and the amount of material wear is reduced accordingly. Figure 7 depicts the evolution of the friction coefficients of the substrate and the cladding layers over time, showing that at the beginning of the wear period, all cladding layers experienced an abrasion phase in which the coefficients of friction gradually climbed up, and then stepped into a relatively smooth wear phase [9]. This is due to the formation of three-body abrasive wear in the contact zone by the hard abrasive chips generated in the initial wear phase, which further aggravates the mechanical interference. Under dry friction, abrasive retention leads to a continuous rise in the friction factor. After wear the actual contact area increases, the unit pressure decreases and the friction changes from adhesion dominated to shear dominated. In the stabilization stage, the particle size of the abrasive debris decreases, part of which is pressed into the surface to form a transfer film, and part of which is discharged through reciprocating motion. At this time, the chip generation rate and discharge rate to reach equilibrium, the friction factor tends to stabilize. It is observed that the friction curve at this time is relatively stable but with some ups and downs, which may be due to the amorphous oxide inclusions such as Cr_2O_3 generated in the cladding process to disrupt the continuity of the amorphous oxide localized flaking, uneven distribution of hard phases, and the cyclic buildup of debris in the process of friction and removal, resulting in late fluctuations in the friction curve.

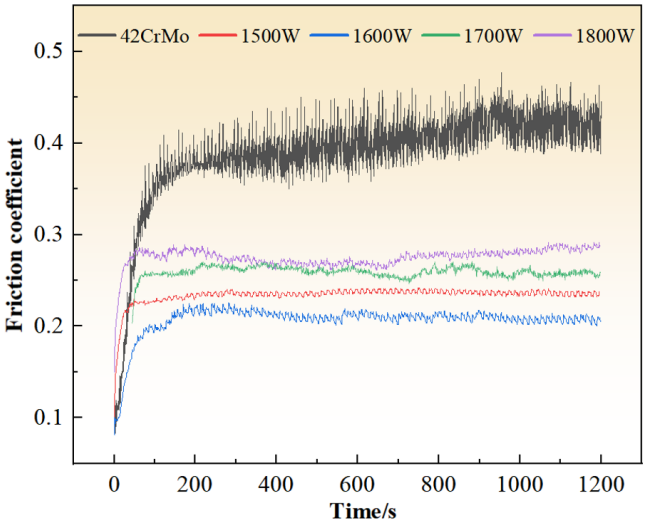

Figure 7. Friction coefficient of the cladding layers

As shown in Figure 8, the wear rates of the 42CrMo steel matrix and each cladding layer were calculated, and the wear rates of the cladding layers were all less than the wear rate of the 42CrMo steel matrix of $4.5\times10^{-2}mm^3/Nm$, with the lowest wear rate of the cladding layer of $1.6\times10^{-2}mm^3/Nm$ at 1600 W, and the lowest wear rate of the cladding layer of $2.3\times10^{-2}mm^3/Nm$, the wear rate test further verified the necessity of process optimization.

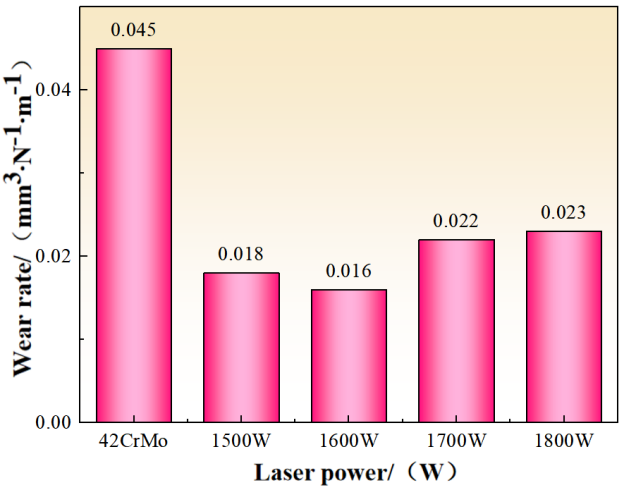

Figure 8. Wear rate of the cladding layers

As shown in Figure 9, the wear morphology of 42CrMo and the cladding layer can be revealed by scanning electron microscopy, which reveals the wear mechanism. The substrate surface shows a continuous plastic deformation band, and a large number of adhesion pits and material migration traces are distributed along the friction direction [10]. At a laser power of 1500 W, the wear surface of the cladding layer shows a significant difference in characteristics: the main wear zone first produces tear lines and localized spalling pits under the effect of stress concentration, while shallow furrows are seen in other wear zones. This morphology suggests that under cyclic stress, the cladding layer first undergoes grain boundary cracking due to dislocation accumulation by fatigue wear, followed by spalling triggered by interfacial detachment by adhesive wear. Only abrasive wear occurs in the unspalled region. When the power is increased to 1600 W, the wear morphology improves significantly: the length of the tear pattern is shortened and the flaking area is reduced. This is because the grain size refinement and higher hard phase content make the crack extension path zigzag, and the stress at the crack tip is weakened, which effectively inhibits the spalling extension. And when more than 1700W, at this time, the surface of the cladding layer spalling phenomenon is serious, coarse grains weaken the grain boundary bonding strength, small area spalling area of epitaxial tearing pattern in the cyclic stress cracks along the coarse dendritic arm rapid expansion, the formation of a continuous crack band. Under the synergistic effect of frictional shear and tensile stress leads to shedding, forming a large area of blocky spalling area.

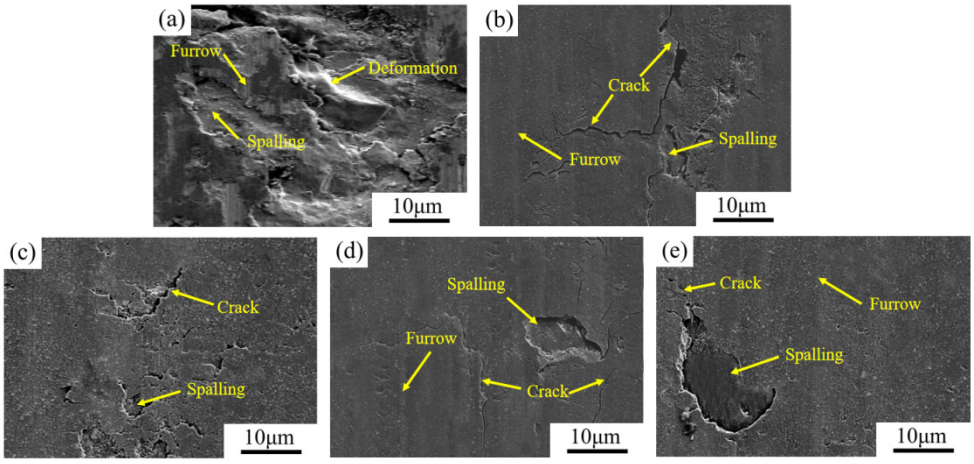

Figure 9. Wear morphology of the cladding layers:
(a) 42CrMo, (b) 1500W, (c) 1600W, (d) 1700W, (e) 1800W

4. CONCLUSION

In this paper, NiCrFeCu-45%WC composite cladding layer is prepared on the surface of 42CrMo steel by laser cladding technology, and the influence of laser power on the organization and properties of the coating is systematically investigated, and the following conclusions are drawn:

(1) the laser power can significantly regulate the composition of the physical phase and grain size of the cladding layer. 1600W, WC partially decomposed to generate W_2C particles, combined with the Zener pinning effect to inhibit grain coarsening, γ-(Ni,Fe) solid solution grain refinement is obvious; after the power of more than 1700W, the cooling rate decreases leading to the coarsening of the dendrites, and the interfacial bonding is weakened.

(2) The hardness of the cladding layer shows a gradient distribution, with the highest hardness at the top due to fine grain strengthening and carbide precipitation, and decreasing towards the substrate due to the dilution effect. the average hardness of the 1600W group reaches 747.6$HV_{1.0}$, which is 1.4 times higher than that of the substrate.

(3) The wear-resistant performance has a non-linear relationship with the power, and the lowest friction coefficient is 0.211 and the lowest wear rate is 1.6×10^{-2} mm^3/Nm at 1600W, which is 64% lower than that of the substrate, and the wear mechanism is dominated by the slight abrasive wear.

CONFLICTS OF INTEREST

The authors declare that they have no known competing financial interests or personal relationships that could have appeared to influence the work reported in this paper.

ACKNOWLEDGMENTS

This work was support by 111 project of China [D21017]; Shandong Provincial Key Research and Development Program (International Science and Technology Cooperation) [No. 2024KJHZ002]; Natural Science Foundation of Shandong Province [No. ZR2023ME156]; Double Hundred Plan" Talent Program of Shandong Province [WSR2023055]; National Natural Science Foundation of China [52405492]; Qingdao Natural Science Foundation [24-4-4-zrjj-68-jch].

REFERENCES

[1] R. Feng, J.D. Pan, J.Z. Zhang, Y.B. Shao, B.S. Chen, Z.Y. Fang, K. Roy, J.B.P. Lim, Effects of corrosion morphology on the fatigue life of corroded Q235B and 42CrMo steels: Numerical modelling and proposed design rules, Structures. 57 (2023) 105136, https://doi.org/10.1016/j.istruc.2023.105136.

[2] G.Y. Sui, X.M. Fang, H.L. Li, X. Wu, C.Z. Zhao, F.C. Jiang, Z.Q. Wang, Cyclic deformation behaviors and microstructure evolution mechanisms of 42CrMo steels under different heat-treatment states, Engineering Failure Analysis. 161 (2024) 108303, https://doi.org/10.1016/j.engfailanal.2024.108303.

[3] C. Guo, J.M. Chen, J.S. Zhou, J.R. Zhao, L.Q. Wang, Y.J. Yu, H.D. Zhou, Effects of WC–Ni content on microstructure and wear resistance of laser cladding Ni-based alloys coating, Surf. Coat. Technol. 206 (8–9) (2012) 2064–2071, https://doi.org/10.1007/s11665-011-0109-8.

[4] J.S. Xu, X.C. Zhang, F.Z. Xuan, Z.D. Wang, S.T. Tu, Microstructure and sliding wear resistance of laser cladded WC/Ni composite coatings with different contents of WC particle, J. Mater. Eng. Perform. 21 (9) (2012) 1904–1911, https://doi.org/10.1016/j.surfcoat.2011.06.005.

[5] Y.H. Zhao, J. Sun, J.F. Li, Study on crack sensitivity and tribological characterisation of functionally gradient material multi-layer by laser cladding with powder mixture of Ni-based alloy and tungsten carbide, Int. J. Surf. Sci. Eng. 9 (4) (2015) 370–383, https://doi.org/10.1504/ijsurfse.2015.070814.

[6] F. Wirth, K. Wegener, A physical modeling and predictive simulation of the laser cladding process, Addit. Manuf. 22 (2018) 307–319, https://doi.org/10.1016/j.optlastec.2020.106784.

[7] W.L. Li, R.F. Di, R.W. Yuan, H.Y. Song, J.B. Lei, Microstructure, wear resistance and electrochemical properties of spherical/non-spherical WC reinforced Inconel 625 superalloy by laser melting deposition, J. Manuf. Process. 74 (2022) 413–422, https://doi.org/10.1016/j.jmapro.2021.12.045.

[8] Q.S. M, Y.J. L, J. W, Effects of ti addition on microstructure homogenization and wear resistance of wide-band laser clad Ni60/WC composite coatings, Int. J. Refract. Met. Hard Mater. 64 (2017) 225–233, https://doi.org/10. 1016/ j.ijrmhm.2016.11.002.

[9] Z.P. Tong, X.D. Ren, W.F. Zhou, S. Adu-Gyamfi, L. Chen, Y.X. Ye, Y.P. Ren, F.Z. Dai, J.D. Yang, L. Li, Effect of laser shock peening on wear behaviors of TC11 alloy at elevated temperature, Optics & Laser Technology. 109 (2019) 139-148, https://doi.org/10.1016/j.optlastec.2018.07.070.

[10] J.B. Liu, Y.L. Huo, J. Xiong, Z.X. Guo, T.E. Yang, J.L. Ye, J.F. Zhao, Y. Liu, Growth and properties of multi-layer nano CrAlN/TiAlN composite coating on the cermets with CrFeCoNiMo, CrFeCoNiMn, CrFeCoNiAl high entropy alloy phase, Appl. Surf. Sci. 572 (2022) 151309, https://doi.org/10.1016/j.apsusc.2021.151309.